ACS APPLIED ENERGY MATERIALS

www.acsaem.org Article

Photoinduced Hole Hopping across CdS Quantum Dot Surfaces for Photoelectrochemical Water Oxidation

Fushuang Niu, Quan Zhou, Rong Liu, and Ke Hu*

Cite This: ACS Appl. Energy Mater. 2022, 5, 1244−1251 Read Online

ACCESS | Metrics & More | Article Recommendations | Supporting Information

ABSTRACT: Water oxidation is typically the rate-limiting half-reaction for water splitting. This is particularly problematic for II-VI materials where chalcogenide oxidation competes favorably with water oxidation. Herein, we introduce and characterize a hybrid quantum dot (QD)-molecular photoanode assembly in which CdS QDs with carbazole-derived hole-transport molecules (HTs) anchoring on the surfaces were immobilized on a mesoporous TiO_2 thin film. Band gap excitation of the CdS QDs resulted in excited state electron transfer to the conduction band of TiO_2 ($k_{inj} > 10^8\ s^{-1}$) as well as hole transfer from the CdS QD to the surface-anchored HT ($k_{HT} > 10^8\ s^{-1}$). Lateral and isoenergetic HT^+/HT "hole transfer" translates the oxidizing equivalents across the CdS QD surface. Transient spectroscopic measurements, as well as Monte Carlo simulations, show that rapid lateral hole hopping across CdS QDs kinetically outcompetes interfacial charge recombination by three orders of magnitude in time. When a molecular water oxidation catalyst was incorporated into the photoanode assembly, HT^+/HT lateral hole hopping resulted in sustained water oxidation. When the HT molecule was present, the faradaic efficiency of water oxidation was threefold larger. Taken together, this study demonstrates that rapid hole transfer of oxidizing equivalents to a catalyst can outcompete photoanodic sulfide oxidation and paves the way for future study of HT-passivated semiconducting materials with favorable band gaps and energetics for water splitting.

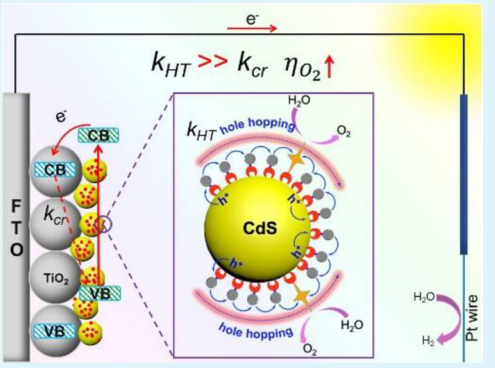

KEYWORDS: *quantum dot, hole hopping, photoelectrochemical cell, water oxidation, transient absorption*

INTRODUCTION

Water oxidation to molecular oxygen often requires the accumulation of four oxidizing equivalents on a single catalytic site. This is a challenging requirement as absorption of one photon typically creates only one oxidizing equivalent.[1,2] Furthermore, the oxidizing equivalents must find the catalytic center before recombination with photogenerated electrons.[3] Fujishima and Honda pioneered this field with the use of a wide band gap semiconductor TiO_2 as both the light absorbing material and the catalyst for solar water oxidation though with limitation on absorption of only the UV part of the solar spectrum.[4] Semiconductor quantum dots (QDs) based on II-VI elements such as CdS or CdSe on the other hand have tunable visible light absorption as well as suitable valence band edge energy for solar water oxidation. Unfortunately, photogenerated holes within unprotected semiconductor nanocrystals favor chalcogenide oxidation rather than water oxidation.[5] Nonetheless, prior studies have managed to mitigate this unwanted photodegradation reaction by applying surface protection layers such as ZnS[6] or NiOOH shells.[7] Another simple way is to transfer photogenerated holes to a molecular water oxidation catalyst either bound on the semiconductor QD surface or codissolved in fluid solution.[8−10] Successfully, an apparent quantum efficiency of 0.27% for solar water splitting as well as hours of sustained oxygen evolution was reported in fluid solution when molecular water oxidation catalysts of ruthenium coordination compounds were linked to CdS nanorods.[10]

The success of using II-VI materials for efficient solar water oxidation while keeping long term stability from chalcogenide oxidation depends on electron/hole transfer kinetics. Prior studies have investigated intensively on the kinetics and dynamics of CdS hole extraction by surface-anchored molecular electron donors. Depending on different electronic coupling or driving forces, the hole extraction kinetic time scale typically spans from a few nanoseconds down to subpicoseconds.[11−13] While ultrafast hole transfer from II-VI materials to molecular electron donors has been suggested to protect from chalcogenide oxidation,[7,10,14] efficient and stable solar water oxidation also relies on retarding the recombination of photogenerated electron−hole pairs and facilitating rapid hole

Received: November 20, 2021
Accepted: December 23, 2021
Published: January 4, 2022

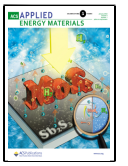

https://doi.org/10.1021/acsaem.1c03651
ACS Appl. Energy Mater. 2022, 5, 1244−1251

Scheme 1. Simplified Interfacial Electron Transfer and Hole Hopping Scheme of the TiO_2|CdS-HT-RubdaS Photoanode Assembly for Photoelectrochemical Water Oxidation

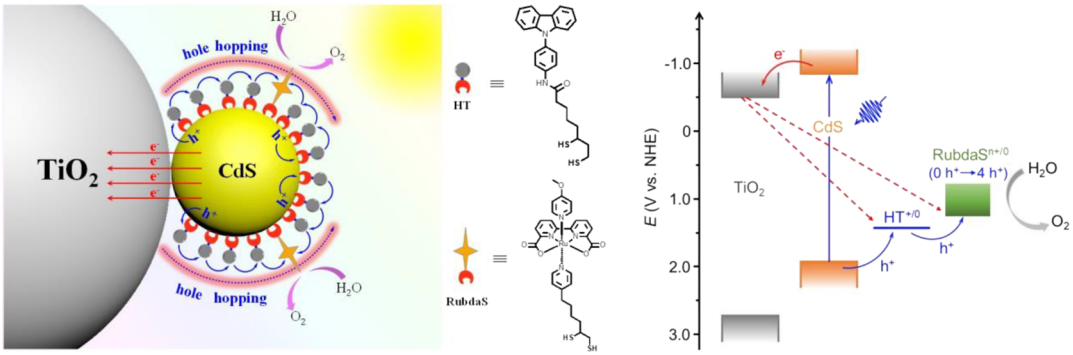

accumulation on the molecular catalytic center.[15] Pervasive early research showed that CdS or CdSe mobile electrons recombined with locally trapped holes on the time scale of a few to hundreds of nanoseconds.[11,16,17] Such rapid recombination falls far short of the catalytic turnover frequency of most champion molecular water oxidation catalysts.[2] Utterback et al., however, reported the observation of diffusive holes on the surfaces of CdS nanorods and suggested a likely advantage of water oxidation through hole mobility that gave rise to rapid hole accumulation to surface-anchored water oxidation catalysts against the dogma of immobile trapped holes incapable of oxidative catalysis for CdS nanocrystals.[14]

Following the guidelines of prior electron/hole transfer kinetics studies based on II-VI nanocrystal materials, we design a new type of molecular-QD hybrid photoanode assembly in which QD surface-attached hole-transport molecules (HTs) play the roles of hole hopping and accumulation to the water oxidation catalyst (WOC). In this assembly, dithiol-functionalized carbazole as the HT and a ruthenium coordination compound (RubdaS) as the WOC were coanchored on the surface of the CdS QD that was immobilized on a mesoporous nanocrystalline (anatase) TiO_2 thin film, Scheme 1. TiO_2 is the electron acceptor while HTs and RubdaS are hole acceptors that extract photogenerated electron−hole pairs from the band gap excitation of CdS QDs. CdS QDs spatially separate TiO_2 and hole acceptors and thereby act not only as the visible light absorber but also the energetic barrier that is supposed to retard interfacial charge recombination. We report the observation of rapid hole extraction and subsequent rapid hole hopping to a molecular catalyst initiated by the band gap excitation of CdS QDs. In the meantime, charge recombination is observed to be about three orders of magnitude slower than hole hopping, which gives remarkably sufficient time for accumulation of four holes[18] on a single molecular catalyst. We illustrate the importance of the HT inclusion on hole hopping kinetics through Monte Carlo simulation and suggest that the semiconductor materials that are known to be unstable under water oxidation conditions can in fact be utilized when rapid hole transfer is operative.

EXPERIMENTAL SECTION

Materials. All chemicals were purchased from Adamas or Beijing Innochem Science & Technology Co., Ltd. and were used as received unless otherwise noted. Fluorine-doped tin oxide (FTO) electrodes (8 Ω/sq) were purchased from Suzhou Shangyang Solar Technology Co. Ltd. Detailed molecular and QD syntheses are provided in the Supporting Information.

Instrumentation and Computation. *Material Characterization.* ^{1}H-NMR and ^{13}C-NMR measurements were performed on a Bruker Avance III HD spectrometer. Transmission electron microscopy (TEM) and field-emission transmission electron microscopy images were taken on Hitachi HT7700 EXALENS and Tecnai G2 F20 S-Twin, respectively. Ground state UV−vis absorption spectra were recorded on an Agilent Cary 60 spectrophotometer.

Nanosecond Transient Absorption Spectroscopy. Nanosecond transient absorption data in the spectral mode were obtained on an Edinburgh LP920 Laser Flash Photolysis system equipped with an ICCD detector (Andor iStar 320T) as was previously described.[19] Briefly, a Q-switched frequency-tripled pulsed Nd:YAG laser (Continuum Surelite I-10) was used to pump an optical parametric oscillator (Continuum, Surelite OPO Plus). A laser excitation wavelength of 430 nm (5−8 nm full width at half-maximum, 1 mJ/cm^2 per pulse) was selected and directed to the sample orthogonally to the white light probe beam generated by a 450 W pulsed xenon lamp. Transient spectral data at each time delay were acquired with typical 20−40 laser pulse averages and were processed with the Edinburgh L900 software. Nanosecond transient absorption data in the kinetic mode were obtained on a TSP-2000 (Unisoku) laser flash photolysis system. A Q-switched frequency-tripled pulsed Nd:YAG laser (Quantel Q-Smart 450, 10 Hz) was used to pump an OPO (OPOTek MagicPrism Inline) to output a laser excitation wavelength of 430 nm (5−8 nm full width at half-maximum, 1 mJ/cm^2 per pulse). A 75 W xenon arc lamp served as the probe beam that was aligned orthogonally to the excitation laser pulse. An R2949 photomultiplier tube (Hamamatsu) coupled to an f/300 mm monochromator (Acton, Princeton Instrument) was used to achieve signal detection. Transient kinetic data at each wavelength were acquired on a logarithmic time scale on a computer interfaced digital oscilloscope (LeCroy 4024, 12 bit, 200 MHz) with typical 50−100 laser pulse averages. Data were processed in Origin 9 and fit with least-squares error minimization using the Levenberg−Marquardt iteration method.

Monte Carlo Simulation. Surface lateral hole hopping kinetics were modeled by Monte Carlo simulation. Monte Carlo runs on the generation of HT^+ and subsequent random hopping until translation of the oxidative equivalent to a catalyst site was repeated 1000 times to achieve a satisfactory signal-to-noise ratio. Simulation codes were implemented in Wolfram Mathematica 11 on a windows PC.

Photoelectrochemical Measurements and O_2 Detection. *Preparation of the Photoelectrodes.* The mesoporous nanocrystalline anatase TiO_2 thin films were prepared according to the previous report.[20] Loading of the CdS QDs and molecular assembly was carried out by immersing the TiO_2 film sequentially in 50 mM 3-mercaptopropionic acid (MPA)-stabilized CdS QD aqueous solutions, HT (5 mM in DCM), 6-(pyridin-4-yl)hexane-1,2-dithiol (Py-2S, 5 mM in DCM), and Ru(2,2′-bipyridine-6,6′-dicarboxylate)-(4-methoxypyridine)$_2$ (Ru(bda)(4-MeOPy)$_2$, 5 mM in MeOH) for 12, 12, 0.5, and 10 h, respectively, to form the photoanode TiO_2|CdS-HT-RubdaS. To help the photoanode surface stability in water, the application of polymethylmethacrylate (PMMA) overlayer coating was carried out on the photoanode TiO_2|CdS-HT-RubdaS by simply

https://doi.org/10.1021/acsaem.1c03651
ACS Appl. Energy Mater. 2022, 5, 1244−1251

Scheme 2. Illustration of the Layer-By-Layer Assembly Procedure for the TiO_2|CdS-HT-RubdaS Photoanode

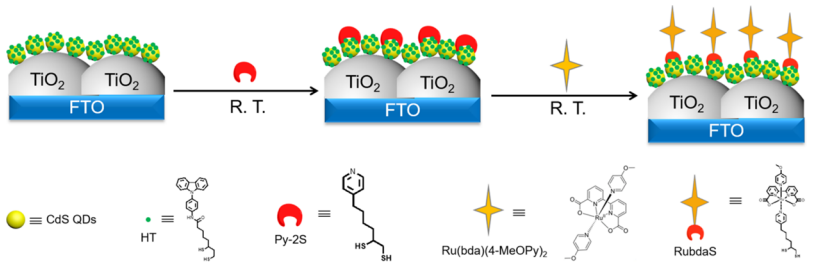

dipping the electrode in dichloromethane (DCM) with 1.0 wt % concentrations of PMMA oligomers. After the electrode was soaked in the DCM/PMMA solution for a few seconds, the film was air-dried.

Photocurrent Measurements and O_2 Detection. Electrochemical and photoelectrochemical experiments were performed using a CH Instruments 760E bipotentiostat. The white light illumination (400 nm cutoff filter, 100 mW/cm^2) was supplied by a Thorlabs HPLS345 light source. The collector-generator experiments for O_2 detection used a four-electrode setup along with a 760E bipotentiostat. Two working electrodes in conjunction with a Pt counter and a Ag/AgCl reference electrode were used. One working (generator) electrode was prepared as described for the photoanode used in the main text; the other working (collector) electrode was plain FTO. Assembly of the collector-generator setup involved placing the two FTO electrodes with the conductive sides facing with narrow 1 mm thick glass spacers between the lateral edges and sealing the sides with epoxy glue (3M), Figure S1. Prepared in this way, the space between the two FTO electrodes will fill with electrolyte by capillary action when the cell is placed in solution. To measure the faradaic efficiency for O_2 production, the charge passed at the generator electrode under the illumination was compared to the total charge passed at the collector electrode (potential bias at −0.85 V vs Ag/AgCl) during the entire experiment. The faradaic efficiency was corrected for the collection efficiency of the same collector-generator setup (70%) (Figure S2) that was determined with a plain FTO (potential bias at +1.60 V vs Ag/AgCl) as the generator electrode and another plain FTO (potential bias at −0.85 V vs Ag/AgCl) as the collector electrode.[21]

RESULTS AND DISCUSSION

Uniformly dispersed 3-mercaptopropionic acid-capped CdS QDs of 3.7 nm diameter in aqueous solution were synthesized according to the literature report, Figure S3.[13] CdS QD-sensitized TiO_2 thin films were prepared by immersing doctor-bladed mesoporous nanocrystalline TiO_2 FTO slides in 0.1 mM CdS QD aqueous solution overnight (concentration determined from the work by Peng and co-workers[22]). Scanning electron microscopy (SEM) with elemental mapping (Figure S4) as well as TEM clearly showed high surface coverage of QDs on TiO_2 nanoparticles of 15−20 nm diameter, Figure S5. The CdS QD-sensitized TiO_2 slide was further dipped in 5 mM HT dichloromethane solution overnight for a maximum surface coverage of ∼9.2 × 10^{-8} mol/cm^2. The QD surface anchoring with HT was presumably from the dithiol linkage to the sulfide surface.[23] The surface coverage of HT on CdS QDs was determined through the absorption peak at 375 nm of oxidized HT generated by the oxidation of the thin film with the oxidant $NOBF_4$ that dissolved CdS off the TiO_2 surface. The same method was used for constructing the Langmuir isotherm for the determination of the equilibrium binding constant of dithiol anchoring to the electrode, Figure S6. The dithiol-functionalized WOC Ru(bda)(PyOMe)(Py2S), where bda is 2,2′-bipyridine-6,6′-dicarboxylic acid, PyOMe 4-methoxy pyridine, and Py2S 6-(pyridin-4-yl)hexane-1,2-dithiol (abbreviated as RubdaS), was loaded onto TiO_2|CdS-HT thin films through an established ligand exchange procedure[24] as pictorially shown in Scheme 2 to afford the photoanode assembly TiO_2|CdS-HT-RubdaS. Finally, a PMMA overlayer was dip-coated (3.0 wt % PMMA solution) onto the photoanode to help photostability as was previously demonstrated effective by Wee et al. and the method was employed thereafter.[25] The ground state absorptions of sensitized thin films are shown in Figure 1.

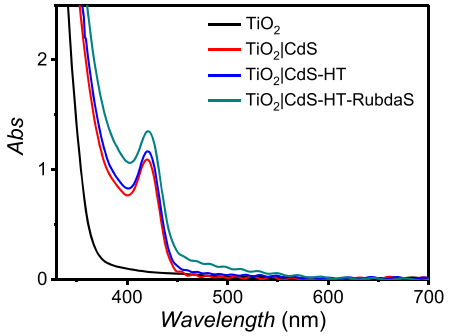

Figure 1. Ground state UV−vis absorption spectra of the TiO_2 thin film (black), CdS QD-sensitized TiO_2 thin film (red), HT-saturated CdS QD-sensitized TiO_2 thin film (blue), and HT-RubdaS-coanchored CdS QD-sensitized TiO_2 thin film (green) photoanode assemblies.

The ratio of the characteristic absorptions at 420 nm over 500 nm determined that eight RubdaSs on average were anchored on a single CdS QD. The calculation detail is shown in the Supporting Information. Molar extinction coefficients for HT in dichloromethane (DCM), HT^+ in DCM, Ru(bda)(4-MeOPy)$_2$ in MeOH, and MPA-coated CdS QDs in sodium bicarbonate aqueous solution (pH ∼ 8.7) are shown in Figure S7.

The layer-by-layer self-assembled TiO_2|CdS-HT-RubdaS was used as the water oxidation photoanode for photocurrent measurement under 100 mW/cm^2 white light irradiation. Under full surface coverage of both CdS and HT, a photocurrent density of 50 μA/cm^2 was obtained at stabilized current, Figure 2A. The initial current spike was assumed to be slow water oxidation catalytic turnover from the catalyst that could not keep up with the charge generation rate and hence a current loss to interfacial charge recombination. When the RubdaS catalyst was absent and hydroquinone (H_2Q) was used as the sacrificial electron donor, the TiO_2|CdS-HT photoanode assembly achieved a photocurrent density of close to 100 μA/cm^2 that was assumed to be the high photocurrent limit for water oxidation. Therefore, the faradaic efficiency for photocatalytic water oxidation was calculated to be about 50−60%. One notable difference of the photoanode assembly apart from other II-VI material-based photoelectrodes was that most

https://doi.org/10.1021/acsaem.1c03651
ACS Appl. Energy Mater. 2022, 5, 1244−1251

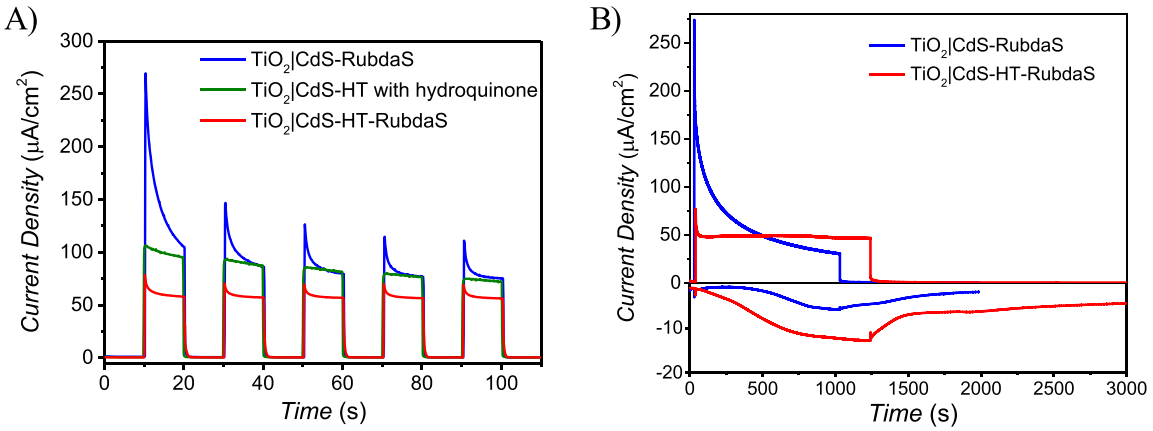

Figure 2. (A) Photocurrent measurements of the indicated photoanode assemblies biased at 0.4 V vs Ag/AgCl reference electrode with 10 s light on and off cycles. (B) Oxygen evolution detection with the collector-generator setup for TiO_2|CdS-RubdaS (blue traces) and TiO_2|CdS-HT-RubdaS (red traces). The upper graph shows the current density profiles for the generator electrodes and the lower graph shows that for the collector electrodes. All the photoelectrodes were illuminated with 100 mW/cm^2 white light equipped with a 400 nm cutoff filter to avoid direct band gap excitation of TiO_2. The electrolyte is 0.5 M Na_2SO_4 and 0.1 M $LiClO_4$ aqueous solution.

CdS or CdSe QDs were used as photocathodes for reductive fuel formations such as proton or CO_2 reduction. Oxidative catalysis was impeded by photocorrosion. Indeed, the photoanode assembly of TiO_2|CdS-RubdaS resulted in much larger photoanodic current (>100 μA/cm^2) but decayed dramatically over time. However, the surface attachment of the redox active carbazole moiety significantly suppressed the current from photocorrosion.

To further investigate that HTs were indeed facilitating catalytic turnover of water oxidation to molecular oxygen, a collector-generator type cell was constructed. The dual working electrodes in which a 1 mm gap was maintained by microscopic glass ensured that the small amount of oxygen gas generated at the photoanode assembly (generator electrode) diffused to the second working electrode (collector electrode) where the oxygen got detected with a forward bias of −0.85 V vs Ag/AgCl. The analytical technique to obtain the faradaic efficiency of oxygen production can be found in the prior study.[21] Figure 2B shows the current density profile for both the generator electrode (upper) and the collector electrode (lower) as a function of time. As light irradiation onto the back of the photoanode was on, the current density from the collector electrode slowly increased as oxygen gas generated from the photoanode got detected. Light irradiation was kept on over 1000 s until current density from the collector electrode plateaued. After the light irradiation was turned off, photocurrent from the photoanode immediately dropped to almost zero while current density from the collector electrode slowly decreased as the remaining oxygen within the gap of the dual working electrodes got consumed.

Although the TiO_2|CdS-HT-RubdaS photoanode assembly initially generated much lower current density than that without HT coadsorption, the current density was well sustained. Furthermore, the collector electrode showed a much higher volume of oxygen generation for the photoanode with full surface coverage of HT as indicated by a larger collector current density. Faradaic efficiency for oxygen production was calculated based on eq 1 where Q_{col}/Q_{gen} is the quotient of the integrated charge from the collector electrode over that from the generator electrode. η_{col} is the correction factor for oxygen collection efficiency that was determined to be 70%. The difference in faradaic efficiencies of oxygen evolution between the photoanodes with and without HT coadsorption was as high as threefold (51.5% vs 14.6%). The faradaic efficiency improvement was attributed to the transfer of photogenerated holes from the valence band of CdS to the surface-anchored HT. Oxidative equivalents on the carbazole moiety were hypothesized to accumulate on surface-anchored RubdaS through lateral intermolecular hole transfer. On the contrary, inefficient hole extraction from oxidized CdS QDs due to the absence of HT and slow catalytic turnover of the WOC resulted in gradual decomposition of CdS QDs similar to the bipyridine ligand loss and hydrolysis triggered from the oxidized ruthenium polypyridyl sensitizers employed in previously reported photoanode assemblies.[26] Another possibility about why unity faradaic efficiency was not achieved based on our current photoanode assembly was because of the dithiol anchoring groups being subject to oxidation. While these anchoring groups are selective toward sulfide surfaces, which the photoanode design was aiming for, they are also known to be easily oxidized.[27]

$$\mathrm{FE} = (Q\mathrm{col}/Q\mathrm{gen})(1/\eta\mathrm{col}) \quad (1)$$

Detailed faradaic efficiency dependence on surface coverage of HT showed that an abrupt increase of faradaic efficiency took place at around 50% of the full surface coverage, Figure 3. Photocurrents from the collector-generator setup are shown in Figure S8. The value of around 50% is in line with the much-studied hole hopping percolation threshold on nanocrystalline TiO_2 surfaces.[28] Although few paid attention to lateral hole hopping on CdS QD surfaces, it is highly likely that lateral hole hopping threshold does not depend much on the substrate to which redox active molecules attach. High surface coverage is a necessity for efficient lateral hole hopping and accumulation to the WOC.

Data from photocurrents as well as oxygen detection through collector-generator measurements clearly indicated the advantage of HT incorporation in a QD-sensitized photoelectrochemical cells. However, HT itself is not catalytic toward water oxidation. It is of great importance to probe the kinetic nature of HTs relaying photogenerated holes to the WOC. Nanosecond transient absorption spectroscopy provided more insights into electron transfer processes of the photoanode assembly followed by the absorption of a photon.

https://doi.org/10.1021/acsaem.1c03651
ACS Appl. Energy Mater. 2022, 5, 1244−1251

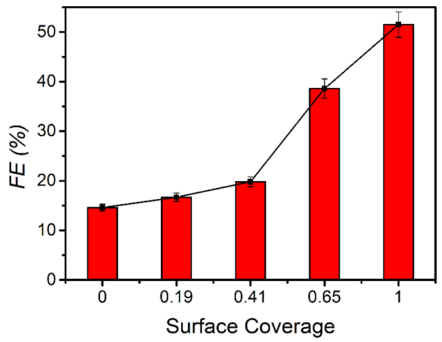

Figure 3. Faradaic efficiencies for photocatalytic water oxidation at variable surface coverages of HTs relative to the full surface coverage of HTs anchored on CdS were calculated from collector-generator measurements based on eq 1 with error bars estimated from three parallel measurements.

A nanosecond laser pulse excitation (5−8 ns FWHM) to the CdS-sensitized TiO_2 film induced an absorption bleach at 430 nm, a positive band at 410 nm, and a positive broad absorption band from 450 nm up to 700 nm, Figure 4A. The transient absorption feature corresponded to a photoinjected electron in the TiO_2 conduction band and a hole left on CdS that recombined over several microseconds, eq 2. Note that a broad positive absorption feature in the whole visible region was persistent over microseconds, which was previously assigned to the trap states close to the valence band of CdS.[11,29] Pulsed laser excitation of the HT-modified CdS-sensitized TiO_2 film resulted in a new absorption peak at around 375 nm, which was captured at 100 ns time delay, Figure 4B. This newly formed spectral signature was in agreement with the photogenerated hole being extracted to the surface-attached HT, eq 3. The holes on HT eventually recombined with $TiO_2(e^-)$s to return to the ground state, eq 4.

$$TiO_2(e^-)|CdS(h^+) \rightarrow TiO_2|CdS \quad (2)$$

$$TiO_2(e^-)|CdS(h^+) - HT \rightarrow TiO_2(e^-)|CdS - HT^+ \quad (3)$$

$$TiO_2(e^-)|CdS - HT^+ \rightarrow TiO_2|CdS - HT \quad (4)$$

Single wavelength kinetic measurement monitored at 375 nm showed that holes at HT persisted over milliseconds, Figure 4C. The nature of the kinetic decay was nonexponential but could be satisfactorily simulated by a stretched exponential function that was widely used for the charge recombination kinetics at the molecular-semiconductor interfaces, eq 5. The beta value was the characteristic stretched exponential factor that was intentionally kept the same for comparative purposes (β = 0.36). By calculating the first moment of the underlying Lévy distribution of the stretched exponential fit, eq 6,[30] the average charge recombination kinetics of $TiO_2(e^-)$ to the oxidized HT was determined to be over two orders of magnitude ($k'_{CR} = 3.7 \times 10^3\ s^{-1}$) slower than that of $TiO_2(e^-)$ to $CdS(h^+)$ ($k_{CR} = 1.1 \times 10^6\ s^{-1}$).

$$\Delta Abs = A \exp[-(kt)^{\beta}] \quad (5)$$

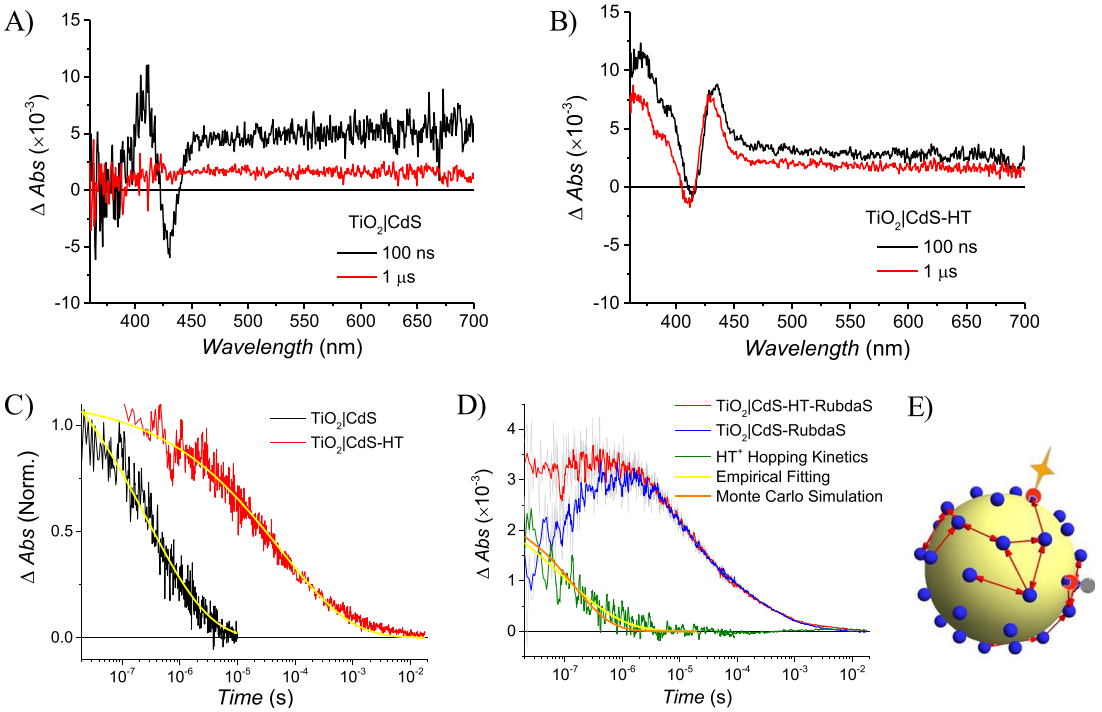

Figure 4. Absorption difference spectra of TiO_2|CdS (A) and TiO_2|CdS-HT (B) at indicated time delays following 430 nm pulsed laser excitation. (C) Normalized delta absorbance changes as a function of time monitored at 410 nm for TiO_2|CdS (black) and at 375 nm for TiO_2|CdS-HT (red). Overlaid in yellow are stretched exponential fits to eq 1. (D) Delta absorbance changes as a function of time monitored at 375 nm for TiO_2|CdS-HT-RubdaS (red) and TiO_2|CdS-RubdaS (blue). The red and blue traces are five-point adjacent averages of the raw data in gray. The green trace representing HT^+ hopping kinetics is the difference between the red and blue traces. Overlaid in yellow is the empirical fitting based on eq 1 and overlaid in orange is the Monte Carlo simulation. (E) Monte Carlo simulation of a representative lateral hole hopping route (red arrows) from HT^+ (gray ball) to a WOC (orange star) based on the random walk model on a spherical CdS nanocrystallite (yellow sphere).

https://doi.org/10.1021/acsaem.1c03651
ACS Appl. Energy Mater. 2022, 5, 1244−1251

$$k_{avg} = \left[\frac{1}{k\beta} \times \Gamma\left(\frac{1}{\beta}\right)\right]^{-1} \quad (6)$$

The retarded interfacial charge recombination could be part of the reason why the incorporation of HT to the QD assembly led to improved faradaic efficiency as was often attributed to for a variety of photoanode assemblies in the literature.[31,32] This is indeed true, but interfacial charge recombination is not the only kinetic factor competing with catalytic turnover. How fast can oxidative equivalents accumulate onto the WOC is also crucial. To study the surface hole accumulation process, the WOC RubdaS was coanchored with HT to the CdS QD to form TiO_2|CdS-HT-RubdaS. The photoanode assembly was subjected to 430 nm pulsed laser excitation. As shown in Figure 4D, a probe wavelength of 375 nm was selected to monitor the absorbance change of HT^+. TiO_2|CdS-RubdaS assembly was used as the reference to account for the other photoinduced absorption changes such as oxidized RubdaS. The absorbance change of HT^+ as a function of time (green trace) was obtained by calculating the absorbance difference between delta absorbance of TiO_2|CdS-HT-RubdaS (red trace) and delta absorbance of TiO_2|CdS-RubdaS (blue trace) both being probed at 375 nm after pulsed 430 nm laser excitation. The instantaneous appearance of the HT^+ signal right after the nanosecond laser pulse was indicative of the fast hole extraction of photoexcited CdS, in accordance with the data shown in Figure 4C. The disappearance of HT^+ occurred from nanoseconds to microseconds and can be ascribed to three electron transfer events that are described in eqs 789.

$$TiO_2(e^-)|CdS - HT^+ - RubdaS \rightarrow TiO_2|CdS - HT - RubdaS \quad (7)$$

$$TiO_2(e^-)|CdS - HT^+ - RubdaS \rightarrow TiO_2(e^-)|CdS - HT - RubdaS^+ \quad (8)$$

$$TiO_2(2e^-)|CdS - HT^+ - RubdaS^+ \rightarrow TiO_2(2e^-)|CdS - HT - RubdaS^{2+} \quad (9)$$

First, HT^+ could recombine with photoinjected electrons in TiO_2 as shown in eq 7. This process is similar to the one shown in eq 4, but the percentage of the process contributing to the loss of HT^+ concentration is probably low as the majority of the interfacial recombination process occurs on the time scale of tens of microseconds to milliseconds. The second electron transfer event could be HT^+ hole hopping to adjacent HT until the oxidative equivalent is collected on RubdaS to form $RubdaS^+$, eq 8. Alternatively, HT^+ could transfer its oxidative equivalent to a $RubdaS^+$ that already obtained an oxidative equivalent from photoexcited CdS as the third possible electron transfer event shown in eq 9. Either event in the second or the third route leading to HT^+ disappearance requires isoenergetic lateral hole hopping among HTs within the same CdS QD on which HTs anchor.

Lateral hole hopping and accumulation as shown in eqs 8 and 9 race against interfacial charge recombination before the photon energy is lost. This hole accumulation process is usually considered the bottleneck for water oxidation. It is of great importance to understand the kinetics of lateral hole hopping and accumulation on the QD photoanode assembly. One way to quantitate the kinetic decay of HT^+ is to use the empirical stretched exponential decay shown in eq 5. The empirical fitting is shown as the yellow curve overlaid on the HT^+ decay data in green. The fitting gives an average rate constant of 3.6×10^6 s^{-1}, which is about three orders of magnitude faster than the interfacial charge recombination shown in Figure 4C. The empirical fitting is useful in that it helps us compare the kinetic data, but it does not provide intrinsic properties of lateral hole hopping.

To glean more insights into this important kinetic process, we performed Monte Carlo simulation on a spherical QD surface where saturation surface coverage of 40 evenly distributed HT and RubdaS molecules in total attach, Figure 4E. The method of constructing such a surface was previously described.[33] The average ratio of HT to RubdaS is four to one based on the ground state absorption of TiO_2|CdS-HT-RubdaS and the ratio is assumed to follow the normal distribution. A random HT obtains a hole from CdS and translates it to one of the RubdaSs through lateral hole hopping. The choice of the next hop is randomly generated with a weighted probability governed by the hole transfer distance. The free energy change ΔG before and after hopping is assumed to be 0 as the hopping is isoenergetic until the hole is trapped to one of the RubdaSs. Then, one Monte Carlo run finishes and the total hopping steps are counted. The hopping time constant is defined as the time spent by the hole waiting on a HT before it translates to another adjacent HT. The hole hopping frequency is simply the inverse of the hopping time constant.

Time-dependent synthetic decays of HT concentrations are compared to the experimental result as the hole hopping frequency (k_{HH}) is varied. The best fit gives $k_{HH} = 1 \times 10^8$ s^{-1} or a hopping time constant (τ_{HH}) of 10 ns/hop. We cannot rule out the possibility of ultrafast hole hopping that was previously observed in a RuP-based photoanode assembly[34] due to the limitation of the instrument time response. Nevertheless, the hopping time constant of 10 ns/hop on a QD sphere is rather rapid considering that a hole could circumnavigate a single QD in less than 100 ns in search of a WOC. In this case, water oxidation will not be limited by hole accumulation and is supposedly only limited by the photon absorption rate of every QD as the interfacial charge recombination is measured to be on the time scale of hundreds of microseconds. In comparison, if a hole circumnavigated a single TiO_2 nanocrystallite of ~15 nm diameter or a network of interconnected nanocrystallites where each has over 500 molecules attached, majority of the hole concentration decay were experimentally determined to occur on the time scale of microseconds to milliseconds in previous reports.[33,35] In such a case, multiple hole accumulation leading to efficient water oxidation will not be expected given such long time scale of hole accumulation with which charge recombination time scale overlaps heavily.

It is unclear whether the lattice structure of the nanocrystallite substrate either CdS or TiO_2 plays a role in the hopping frequency. However, a recent Monte Carlo simulation study comparing four types of particle assembly models for surface hole hopping suggests that the catalytic turnover yield is indeed higher for isolated particles than for heavily overlapped particles as rodlike substrates under certain surface coverages.[36] In this study, CdS QDs can be viewed as isolated particle substrates with much fewer hopping sites than interconnected TiO_2 nanoparticle networks. It is possible

https://doi.org/10.1021/acsaem.1c03651
ACS Appl. Energy Mater. 2022, 5, 1244−1251

that site isolation facilitates surface hole accumulation. Another important factor is the molecular nature of the HT molecule that is capable of rapid hole hopping. Analogous organic molecules such as triphenylamines do show this property compared with ruthenium coordination compounds.[37] Regardless, the HTs indeed help WOCs extract photogenerated holes from CdS QDs and can translate them efficiently to WOCs against the odds of interfacial charge recombination. It is also worth noting that a typical TiO_2|RuP-Rubda-coanchored photoanode assembly reported in the literature could not achieve significant photocurrent and high faradaic efficiency[34,38] unless it was considerably modified to retard interfacial charge recombination or enhance the rate of hole accumulation through core−shell structures, covalent linkages, etc.[31,39,40] The novel QD photoanode assembly studied herein directly improves the two critical kinetic factors through QDs, establishing the energetic barrier for charge recombination between TiO_2 electrons and oxidative equivalents on surface-anchored molecules as well as the efficient HT^+/HT hole hopping across the QD surfaces.

CONCLUSIONS

In conclusion, a new photoanode assembly design was proposed and successfully tested. CdS QDs with a surface-linked carbazole derivatized HT molecule were shown to photo-oxidize water with a faradaic efficiency of 0.51. In the absence of the HT, the faradaic efficiency decreased by a factor of 3. Experimental and Monte Carlo simulations showed that rapid hole transfer, $k_{HH} = 1 \times 10^8\ s^{-1}$ between adjacent carbazole molecules translated the oxidizing equivalents to the WOC with an average kinetic rate constant that was three orders of magnitude faster than the unwanted charge recombination reaction. The new photoanode assembly demonstrates that the bottleneck of sluggish hole accumulation for efficient solar water oxidation can be tackled with separate light harvesting and hole hopping molecules that communicate electronically yet independently perform these tasks. The data also reveal that the water oxidation efficiency of a II-VI semiconductor can be greatly improved through this approach suggesting that it may be extended to other semiconducting materials.

ASSOCIATED CONTENT

Supporting Information

The Supporting Information is available free of charge at https://pubs.acs.org/doi/10.1021/acsaem.1c03651.

Synthesis, experimental details, electron microscopy images, HT surface coverage-dependent faradaic efficiencies, and NMR spectra of relevant molecules (PDF)

AUTHOR INFORMATION

Corresponding Author

Ke Hu − *Department of Chemistry and Shanghai Key Laboratory of Molecular Catalysis and Innovative Materials, Fudan University, Shanghai 200433, P. R. China;* orcid.org/0000-0002-0240-7192; Email: khu@fudan.edu.cn

Authors

Fushuang Niu − *Department of Chemistry and Shanghai Key Laboratory of Molecular Catalysis and Innovative Materials, Fudan University, Shanghai 200433, P. R. China*

Quan Zhou − *Department of Chemistry and Shanghai Key Laboratory of Molecular Catalysis and Innovative Materials, Fudan University, Shanghai 200433, P. R. China*

Rong Liu − *Department of Chemistry and Shanghai Key Laboratory of Molecular Catalysis and Innovative Materials, Fudan University, Shanghai 200433, P. R. China*

Complete contact information is available at: https://pubs.acs.org/10.1021/acsaem.1c03651

Notes

The authors declare no competing financial interest.

ACKNOWLEDGMENTS

This work is sponsored by the National Key R&D Program of China (2018YFE0201701), the National Natural Science Foundation of China (21872037), and the Natural Science Foundation of Shanghai (21ZR1404400). K.H. is particularly grateful to Professor Mingtian Zhang at Tsinghua University for the generous access to his lab's transient absorption apparatus at the early stages of this work. K.H. also thanks Professor Gerald Meyer at UNC Chapel Hill for valuable discussion during preparation of the manuscript.

REFERENCES

(1) Hammarström, L. Accumulative Charge Separation for Solar Fuels Production: Coupling Light-Induced Single Electron Transfer to Multielectron Catalysis. *Acc. Chem. Res.* **2015**, *48*, 840−850.

(2) Zhang, B.; Sun, L. Artificial photosynthesis: opportunities and challenges of molecular catalysts. *Chem. Soc. Rev.* **2019**, *48*, 2216−2264.

(3) Brennaman, M. K.; Dillon, R. J.; Alibabaei, L.; Gish, M. K.; Dares, C. J.; Ashford, D. L.; House, R. L.; Meyer, G. J.; Papanikolas, J. M.; Meyer, T. J. Finding the Way to Solar Fuels with Dye-Sensitized Photoelectrosynthesis Cells. *J. Am. Chem. Soc.* **2016**, *138*, 13085−13102.

(4) Fujishima, A.; Honda, K. Electrochemical Photolysis of Water at a Semiconductor Electrode. *Nature* **1972**, *238*, 37−38.

(5) Nasir, J. A.; Rehman, Z. u.; Shah, S. N. A.; Khan, A.; Butler, I. S.; Catlow, C. R. A. Recent developments and perspectives in CdS-based photocatalysts for water splitting. *J. Mater. Chem. A* **2020**, *8*, 20752−20780.

(6) Yang, H. B.; Miao, J.; Hung, S.-F.; Huo, F.; Chen, H. M.; Liu, B. Stable Quantum Dot Photoelectrolysis Cell for Unassisted Visible Light Solar Water Splitting. *ACS Nano* **2014**, *8*, 10403−10413.

(7) Chen, W.; Huang, G.-B.; Song, H.; Zhang, J. Efficient and stable charge transfer channels for photocatalytic water splitting activity of CdS without sacrificial agents. *J. Mater. Chem. A* **2020**, *8*, 20963−20969.

(8) Pearce, O. M.; Duncan, J. S.; Damrauer, N. H.; Dukovic, G. Ultrafast Hole Transfer from CdS Quantum Dots to a Water Oxidation Catalyst. *J. Phys. Chem. C* **2018**, *122*, 17559−17565.

(9) Tseng, H.-W.; Wilker, M. B.; Damrauer, N. H.; Dukovic, G. Charge Transfer Dynamics between Photoexcited CdS Nanorods and Mononuclear Ru Water-Oxidation Catalysts. *J. Am. Chem. Soc.* **2013**, *135*, 3383−3386.

(10) Wolff, C. M.; Frischmann, P. D.; Schulze, M.; Bohn, B. J.; Wein, R.; Livadas, P.; Carlson, M. T.; Jäckel, F.; Feldmann, J.; Würthner, F.; Stolarczyk, J. K. All-in-one visible-light-driven water splitting by combining nanoparticulate and molecular co-catalysts on CdS nanorods. *Nat. Energy* **2018**, *3*, 862−869.

(11) Wu, K.; Du, Y.; Tang, H.; Chen, Z.; Lian, T. Efficient Extraction of Trapped Holes from Colloidal CdS Nanorods. *J. Am. Chem. Soc.* **2015**, *137*, 10224−10230.

(12) Ding, T. X.; Olshansky, J. H.; Leone, S. R.; Alivisatos, A. P. Efficiency of Hole Transfer from Photoexcited Quantum Dots to

Covalently Linked Molecular Species. *J. Am. Chem. Soc.* **2015**, *137*, 2021−2029.
(13) Lian, S.; Weinberg, D. J.; Harris, R. D.; Kodaimati, M. S.; Weiss, E. A. Subpicosecond Photoinduced Hole Transfer from a CdS Quantum Dot to a Molecular Acceptor Bound Through an Exciton-Delocalizing Ligand. *ACS Nano* **2016**, *10*, 6372−6382.
(14) Utterback, J. K.; Grennell, A. N.; Wilker, M. B.; Pearce, O. M.; Eaves, J. D.; Dukovic, G. Observation of trapped-hole diffusion on the surfaces of CdS nanorods. *Nat. Chem.* **2016**, *8*, 1061−1066.
(15) Tkaczibson, K.; Ardo, S. Numerical Monte Carlo simulations of charge transport across the surface of dye and cocatalyst modified spherical nanoparticles under conditions of pulsed or continuous illumination. *Sustainable Energy Fuels* **2019**, *3*, 1573−1587.
(16) Jones, M.; Lo, S. S.; Scholes, G. D. Quantitative modeling of the role of surface traps in CdSe/CdS/ZnS nanocrystal photoluminescence decay dynamics. *Proc. Natl. Acad. Sci. U. S. A.* **2009**, *106*, 3011−3016.
(17) Peterson, M. D.; Cass, L. C.; Harris, R. D.; Edme, K.; Sung, K.; Weiss, E. A. The Role of Ligands in Determining the Exciton Relaxation Dynamics in Semiconductor Quantum Dots. *Annu. Rev. Phys. Chem.* **2014**, *65*, 317−339.
(18) Lebedev, D.; Pineda-Galvan, Y.; Tokimaru, Y.; Fedorov, A.; Kaeffer, N.; Copéret, C.; Pushkar, Y. The Key RuV=O Intermediate of Site-Isolated Mononuclear Water Oxidation Catalyst Detected by in Situ X-ray Absorption Spectroscopy. *J. Am. Chem. Soc.* **2018**, *140*, 451−458.
(19) Yong, W.-W.; Lu, H.; Li, H.; Wang, S.; Zhang, M.-T. Photocatalytic Hydrogen Production with Conjugated Polymers as Photosensitizers. *ACS Appl. Mater. Interfaces* **2018**, *10*, 10828−10834.
(20) Wang, D.; Sheridan, M. V.; Shan, B.; Farnum, B. H.; Marquard, S. L.; Sherman, B. D.; Eberhart, M. S.; Nayak, A.; Dares, C. J.; Das, A. K.; Bullock, R. M.; Meyer, T. J. Layer-by-Layer Molecular Assemblies for Dye-Sensitized Photoelectrosynthesis Cells Prepared by Atomic Layer Deposition. *J. Am. Chem. Soc.* **2017**, *139*, 14518−14525.
(21) Sherman, B. D.; Sheridan, M. V.; Dares, C. J.; Meyer, T. J. Two Electrode Collector−Generator Method for the Detection of Electrochemically or Photoelectrochemically Produced O2. *Anal. Chem.* **2016**, *88*, 7076−7082.
(22) Yu, W. W.; Qu, L.; Guo, W.; Peng, X. Experimental Determination of the Extinction Coefficient of CdTe, CdSe, and CdS Nanocrystals. *Chem. Mater.* **2003**, *15*, 2854−2860.
(23) Han, Z.; Qiu, F.; Eisenberg, R.; Holland, P. L.; Krauss, T. D. Robust Photogeneration of H₂ in Water Using Semiconductor Nanocrystals and a Nickel Catalyst. *Science* **2012**, *338*, 1321−1324.
(24) Wang, D.; Marquard, S. L.; Troian-Gautier, L.; Sheridan, M. V.; Sherman, B. D.; Wang, Y.; Eberhart, M. S.; Farnum, B. H.; Dares, C. J.; Meyer, T. J. Interfacial Deposition of Ru(II) Bipyridine-Dicarboxylate Complexes by Ligand Substitution for Applications in Water Oxidation Catalysis. *J. Am. Chem. Soc.* **2018**, *140*, 719−726.
(25) Wee, K.-R.; Brennaman, M. K.; Alibabaei, L.; Farnum, B. H.; Sherman, B.; Lapides, A. M.; Meyer, T. J. Stabilization of Ruthenium(II) Polypyridyl Chromophores on Nanoparticle Metal-Oxide Electrodes in Water by Hydrophobic PMMA Overlayers. *J. Am. Chem. Soc.* **2014**, *136*, 13514−13517.
(26) Hyde, J. T.; Hanson, K.; Vannucci, A. K.; Lapides, A. M.; Alibabaei, L.; Norris, M. R.; Meyer, T. J.; Harrison, D. P. Electrochemical Instability of Phosphonate-Derivatized, Ruthenium-(III) Polypyridyl Complexes on Metal Oxide Surfaces. *ACS Appl. Mater. Interfaces* **2015**, *7*, 9554−9562.
(27) Abdellah, M.; Zhang, S.; Wang, M.; Hammarström, L. Competitive Hole Transfer from CdSe Quantum Dots to Thiol Ligands in CdSe-Cobaloxime Sensitized NiO Films Used as Photocathodes for H2 Evolution. *ACS Energy Lett.* **2017**, *2*, 2576−2580.
(28) Bonhôte, P.; Gogniat, E.; Tingry, S.; Barbé, C.; Vlachopoulos, N.; Lenzmann, F.; Comte, P.; Grätzel, M. Efficient Lateral Electron Transport inside a Monolayer of Aromatic Amines Anchored on Nanocrystalline Metal Oxide Films. *J. Phys. Chem. B* **1998**, *102*, 1498−1507.
(29) Wu, K.; Zhu, H.; Liu, Z.; Rodríguez-Córdoba, W.; Lian, T. Ultrafast Charge Separation and Long-Lived Charge Separated State in Photocatalytic CdS−Pt Nanorod Heterostructures. *J. Am. Chem. Soc.* **2012**, *134*, 10337−10340.
(30) Lindsey, C. P.; Patterson, G. D. Detailed comparison of the Williams–Watts and Cole–Davidson functions. *J. Chem. Phys.* **1980**, *73*, 3348−3357.
(31) Wee, K.-R.; Sherman, B. D.; Brennaman, M. K.; Sheridan, M. V.; Nayak, A.; Alibabaei, L.; Meyer, T. J. An aqueous, organic dye derivatized SnO2/TiO2 core/shell photoanode. *J. Mater. Chem. A* **2016**, *4*, 2969−2975.
(32) Xu, P.; Gray, C. L.; Xiao, L.; Mallouk, T. E. Charge Recombination with Fractional Reaction Orders in Water-Splitting Dye-Sensitized Photoelectrochemical Cells. *J. Am. Chem. Soc.* **2018**, *140*, 11647−11654.
(33) Hu, K.; Robson, K. C. D.; Beauvilliers, E. E.; Schott, E.; Zarate, X.; Arratia-Perez, R.; Berlinguette, C. P.; Meyer, G. J. Intramolecular and Lateral Intermolecular Hole Transfer at the Sensitized TiO2 Interface. *J. Am. Chem. Soc.* **2014**, *136*, 1034−1046.
(34) Grądzka-Kurzaj, I.; Gierszewski, M.; Timmer, B. J. J.; Ziółek, M. Molecular Water Oxidation Catalysis: Characterization of Subnano-second Processes and Ruthenium "Green Dimer" Formation. *ACS Appl. Energy Mater.* **2021**, *4*, 2440−2450.
(35) Chen, H.-Y.; Ardo, S. Direct observation of sequential oxidations of a titania-bound molecular proxy catalyst generated through illumination of molecular sensitizers. *Nat. Chem.* **2018**, *10*, 17−23.
(36) Tkaczibson, K.; Ardo, S. Numerical Monte Carlo Simulations to Evaluate the Influence That Spherical Nanoparticle Size and Arrangement Have on Interparticle Charge Transport across the Surface of Dye- and Cocatalyst-Modified Materials. *ACS Appl. Energy Mater.* **2020**, *3*, 4699−4707.
(37) Hu, K.; Meyer, G. J. Lateral Intermolecular Self-Exchange Reactions for Hole and Energy Transport on Mesoporous Metal Oxide Thin Films. *Langmuir* **2015**, *31*, 11164−11178.
(38) Song, W.; Ito, A.; Binstead, R. A.; Hanson, K.; Luo, H.; Brennaman, M. K.; Concepcion, J. J.; Meyer, T. J. Accumulation of Multiple Oxidative Equivalents at a Single Site by Cross-Surface Electron Transfer on TiO2. *J. Am. Chem. Soc.* **2013**, *135*, 11587−11594.
(39) Sherman, B. D.; Xie, Y.; Sheridan, M. V.; Wang, D.; Shaffer, D. W.; Meyer, T. J.; Concepcion, J. J. Light-Driven Water Splitting by a Covalently Linked Ruthenium-Based Chromophore−Catalyst Assembly. *ACS Energy Lett.* **2017**, *2*, 124−128.
(40) Alibabaei, L.; Sherman, B. D.; Norris, M. R.; Brennaman, M. K.; Meyer, T. J. Visible photoelectrochemical water splitting into H2 and O2 in a dye-sensitized photoelectrosynthesis cell. *Proc. Natl. Acad. Sci. U. S. A.* **2015**, *112*, 5899−5902.

https://doi.org/10.1021/acsaem.1c03651
ACS Appl. Energy Mater. 2022, 5, 1244−1251